Sulfoxidation Mechanisms Catalyzed by Cytochrome P450 and Horseradish Peroxidase Models: Spin Selection Induced by the Ligand[†,‡]

Devesh Kumar,[§] Sam P. de Visser,[||] Pankaz K. Sharma,[§] Hajime Hirao,[§] and Sason Shaik*[,§]

Department of Organic Chemistry and the Lise Meitner-Minerva Center for Computational Quantum Chemistry, The Hebrew University of Jerusalem, 91904 Jerusalem, Israel, and School of Chemical Engineering and Analytical Science, University of Manchester, PO Box 88, Sackville Street, Manchester M60 1QD, U.K.

Received February 24, 2005; Revised Manuscript Received April 2, 2005

ABSTRACT: The sulfoxidation of dimethyl sulfide (DMS), by two different heme-type enzyme models (without the protein), namely, horseradish peroxidase (HRP) and cytochrome P450 (P450), was studied using density functional theory. The models differ from each other by the axial ligand of the iron, which is imidazole in the case of HRP and thiolate in the case of P450. The computational results reveal *a concerted oxygen atom transfer to sulfur, with spin-state selection dependent upon the identity of the proximal ligand*. In the case of thiolate, the mechanism prefers the high-spin quartet pathway; whereas in the case of imidazole, the mechanism involves two-state reactivity (TSR), with competing quartet and doublet spin states. Furthermore, with thiolate the high-spin transition state, ^{4}**TS**$_{P450}$, has an upright conformation with a large Fe−O−S_{DMS} angle of 147°, whereas the low-spin species, ^{2}**TS**$_{P450}$, has a small angle and its Fe−O moiety makes an O−N_{Por} bond with one of the nitrogen atoms of the porphine macrocycle. By contrast, when the proximal ligand is imidazole, both transition states possess a bent Fe−O bond and an O−N_{Por} bond. These spin-state selection patterns *obey simple orbital-selection rules*, which are manifestations of the electronic nature of the ligand, i.e., the electron-releasing effect of the thiolate vis-à-vis the electron-withdrawal effect of imidazole. Other possible reactivity expressions of the spin-selection patterns are discussed [Dowers, T. S., Rock, D. A., Rock, D. A., Jones, J. P. (2004) *J. Am. Chem. Soc. 126*, 8868−8869]. Theory shows that *intrinsically*, HRP should be as reactive as P450 toward sulfoxidation.

Heme-enzymes share the same active-species type, but nevertheless they tend to exhibit a great many differences in electronic properties and reactivity (*1*−*8*). Two of these heme-enzymes are cytochrome P450 (P450[1]) and horseradish peroxidase (HRP); both utilize as the active species a high-valent oxo−iron heme species, called compound I (Cpd I). As illustrated in Scheme 1, using the crystal structures of Schlichting et al. (*9*) and Berglund et al. (*10*), an essential difference of these two enzymes is the axial ligand (so-called proximal ligand) bound to the iron; P450 has a thiolate proximal ligand of a cysteinate side chain, whereas HRP binds an imidazole group of a histidine side chain. Since cysteinate is an anionic ligand while histidine is neutral, the different interactions of the ligands with the metal are likely to tune the electronic properties of the active species. In particular, the electron-donating power of cysteinate makes the heme a poorer electron acceptor (*11*−*13*), compared with the histidine heme in HRP. Thus, HRP generally functions as an electron sink and participates in electron-transfer mechanisms. Indeed, a recent theoretical estimate (*14*) showed that the electron affinity of Cpd I (HRP) is 6.41 eV, well over 3 eV higher than Cpd I (P450). Still, though, the ground state of the active species, Cpd I, in both cases is the same state type, being a triradicaloid with unpaired

Scheme 1: The Active Sites and Differences in Active-Site Structure of HRP (PDB code 1HCH (*10*), Left) and the Putative Species of P450 (PDB code 1DZ9 (*9*), Right) with Critical Amino Acid Residues and Water Molecules Labeled as W

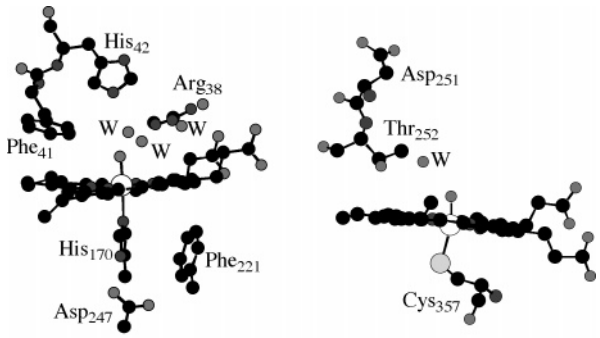

[†] The research at the HU was supported by a grant to S.S. from the BMBF-DIP (Grant No. DIP-G.7.1). The University of Manchester is acknowledged for support of S.P. de V.

[‡] Dedicated to P. v. R. Schleyer, a great scientist and a friend, on his forthcoming 75th birthday.

* To whom correspondence should be addressed. Tel: +972-2-6585909. Fax: +972-2-6584680. E-mail: sason@yfaat.ch.huji.ac.il.

[§] The Hebrew University of Jerusalem.

[||] University of Manchester.

[1] Abbreviations: DMS, dimethyl sulfide; HRP, horseradish peroxidase; P450, cytochrome P450; TSR, two-state reactivity; SSR, single-state reactivity; Cpd I, compound I; PDB, Protein Data Bank; Mb, myoglobin; DFT, density functional theory; SH^-, thiolate ligand; ImH, imidazole ligand; TS, transition state; HS, high-spin; LS, low-spin; ZPE, zero-point energy; Por, porphine.

10.1021/bi050348c CCC: $30.25
Published on Web 05/13/2005

electrons in two π^* orbitals along the Fe−O bond and one in a porphyrin-based orbital (*14*−*24*). One would therefore like to understand and predict the different *intrinsic* reactivity patterns elicited by the two ligand types, without the influence of the protein. This is the main goal of the present paper.

Although HRP functions predominantly as an electron sink (*4*, *8*, *25*), it is also known to perform oxygen-transfer reactions (*26*−*32*). Generally, however, the reactivity of HRP enzymes is sluggish compared with P450 enzymes; sulfoxidation is the most efficient while C−H hydroxylation is rather inefficient. This sluggishness is thought to originate mainly in the much smaller substrate-binding pocket in HRP (*4*, *25*, *28*−*30*). As can be seen from Scheme 1, bulky amino acid residues such as Arg_{38}, Phe_{41}, and His_{42} occupy the active pocket, thereby preventing large substrates from entering the active site. HRP mutants, like the Phe41Leu mutant, with a larger substrate binding pocket exhibited indeed enhanced reactivity toward sulfoxidation and in some cases even gave enantioselective products (*28a*,*b*). Other histidine-linked heme enzymes, such as myoglobin (Mb), also perform oxygen-transfer reactions, although native Mb is actually an oxygen transport heme-protein (*33*). Myoglobin mutants with either peroxidase-like or P450-like active sites exhibit enhanced reactivity toward sulfoxidation (*33*−*35*). Studies of model compounds (*36*−*38*) showed that synthetic imidazole- and thiolate-ligated iron porphyrins are capable of acting as monooxygenating catalysts, but the relative reactivity toward hydroxylation and epoxidation is different and depends on the axial ligand. Since this is generally the case also for the enzymes themselves (*28*, *29*, *39*, *40*), it seems that while both Cpd I types may be intrinsically capable of oxygenating organic compounds, one might expect different chemoselectivity depending on the axial ligand. Accordingly, the key question of the present paper concerns the issue of the different intrinsic reactivity of the two species. To treat this issue on equal footing, for P450 vs HRP, we decided to focus on the mechanism of sulfur oxidation, i.e., sulfoxidation, and use density functional theory (DFT) to delineate the mechanism of this process for the two Cpd I models.

Two hypotheses have been proposed for the reaction mechanism of sulfoxidation by HRP (*31*). The first one involves direct oxygen transfer from Cpd I to the RSR′ substrate. An alternative mechanism suggests initial electron transfer from the substrate to Cpd I followed by oxygen atom transfer from the reduced species of Cpd I, so-called Cpd II, to form the products. Oxygen transfer from the solvent was ruled out since ^{18}O labeling showed that one of the oxygen atoms of $H_2{}^{18}O_2$, i.e., the oxygen atom of Cpd I, is transferred to the substrate (*27*, *41*). Since the substrate binding pocket of HRP is fairly small (*29*), it was generally concluded that the reaction proceeds via an initial electron transfer from the substrate (alkyl sulfide) to Cpd I. Goto et al. (*31*) estimated the efficiency of the rebound of the electron-transferred substrate to be ca. 25%; the remainder of the alkyl sulfide cation radicals is expected to diffuse from the cage without oxygen uptake. These mechanistic hypotheses will be tested in the present theoretical study, which to the best of our knowledge constitutes one of the first theoretical comparisons of the reactivity of the two "bare" species (*42*).

COMPUTATIONAL METHODS

The calculations presented here follow procedures similar to those employed by the group before (*14*, *43*, *44*). The Cpd I species were modeled using an oxo−iron porphine without side chains, and a thiolate (SH^-) axial ligand in the case of P450 and an imidazole (ImH) ligand in the case of HRP (*14*, *45*). Our recent investigation of Cpd I (HRP) (*14*), which included imidazole and aspartate as well as the side chain of Phe (Scheme 1), showed that while there is a hydrogen bond between imidazole and aspartate, the resulting imidazolate character and the extent of spin density on the ligand are small; when the effect of a dielectric medium is included, most of the spin density resides on the porphyrin. Following this study, an imidazole ligand is deemed a better representation of the proximal ligand than imidazolate. As such, since ImH is a neutral ligand, whereas SH^- is an anionic ligand, the total charge of the Cpd I (HRP) species is +1 while that of Cpd I (P450) is zero. Following our previous communication on the sulfoxidation by P450 model Cpd I, we used dimethyl sulfide (DMS) as a substrate (*46*).

All calculations used the unrestricted hybrid density functional method UB3LYP (*47*). The calculations with Cpd I (P450) were performed before (*43*, *44*) with the Gaussian 98 (*48*) and Jaguar 4.2 (*49*) program packages for both geometry optimizations and frequency calculations and used the LACVP** basis set on iron and the 6-31G** basis set on the remaining atoms, in a brief notation LACVP** (*50*). The same basis set was used here for the reaction of Cpd I (HRP) with DMS. The relative energies of the transition states were improved with larger basis sets up to LACV3P++**, which is a triple-ζ basis set with polarization and diffuse functions on all atoms. Quite a few of these results are relegated to the Supporting Information, along with other data produced during the study.

All local minima presented here had real frequencies, while the transition states were characterized with a single imaginary frequency of the correct reaction eigenmode. The effect of the environment was studied using the self-consistent reaction field (SCRF) method as implemented in Jaguar 4.2 (*49*) with a dielectric constant of $\epsilon = 5.708$ and a probe radius of 2.72 Å.

RESULTS

Key Orbitals in HRP and P450 Cpd I. Scheme 2 displays the high-lying occupied and low-lying virtual orbitals of Cpd I (HRP). Alongside each other are shown the "a_{2u}" orbitals of Cpd I (HRP) and Cpd I (P450), which are the main distinguishing orbitals between the two species. The two species share a set of d-type orbitals, which include the nonbonding δ-orbital, the antibonding Fe=O orbitals, $\pi^*_{xz,yz}$, the antibonding Fe−N_{Por} interactions (σ^*_{xy}), and the antibonding proximal ligand−Fe−O ($\sigma^*_{z^2}$). The remaining orbital, "a_{2u}", is considerably different. In Cpd I (HRP) it is virtually a pure porphyrin orbital with little or no mixing from the ligand. By contrast, in Cpd I (P450), a_{2u} mixes strongly with the lower-lying σ_S orbital of the thiolate ligand and becomes the corresponding antibonding combination ($a_{2u} - \sigma_S$), shown as "a_{2u} (P450)" in Scheme 2 (the bonding combination, ($a_{2u} + \sigma_S$), is low lying and doubly occupied). Since the "a_{2u} (P450)" orbital is raised in energy by the mixing with the sulfur orbital, the electron affinity of Cpd I

Scheme 2: Key Orbitals of Cpd I of HRP[a]

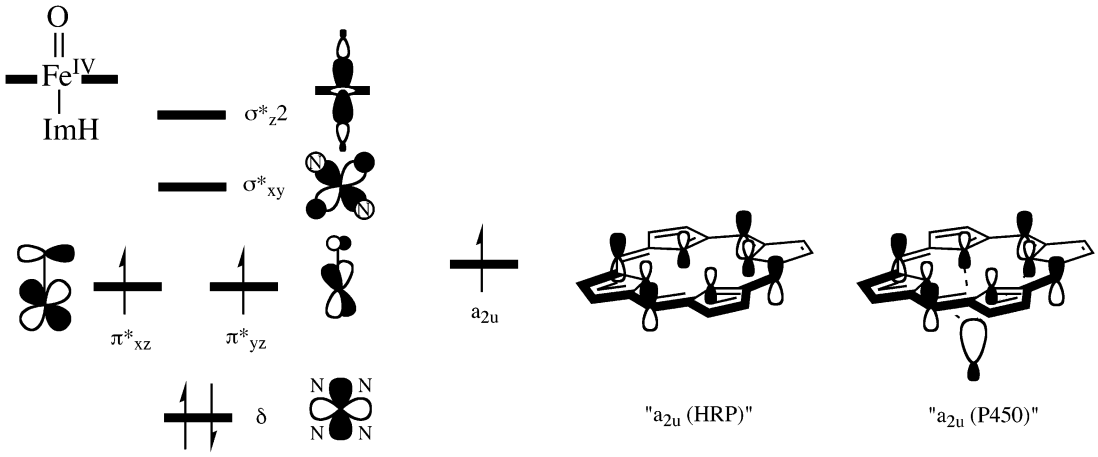

[a] The "a_{2u}" orbitals of Cpd I (HRP) and Cpd I (P450) are drawn alongside each other for comparison. The orbital occupancy corresponds to the quartet spin state. In the doublet state, the a_{2u} electron spin is opposite to the two spins of the π^* electrons on the FeO moiety.

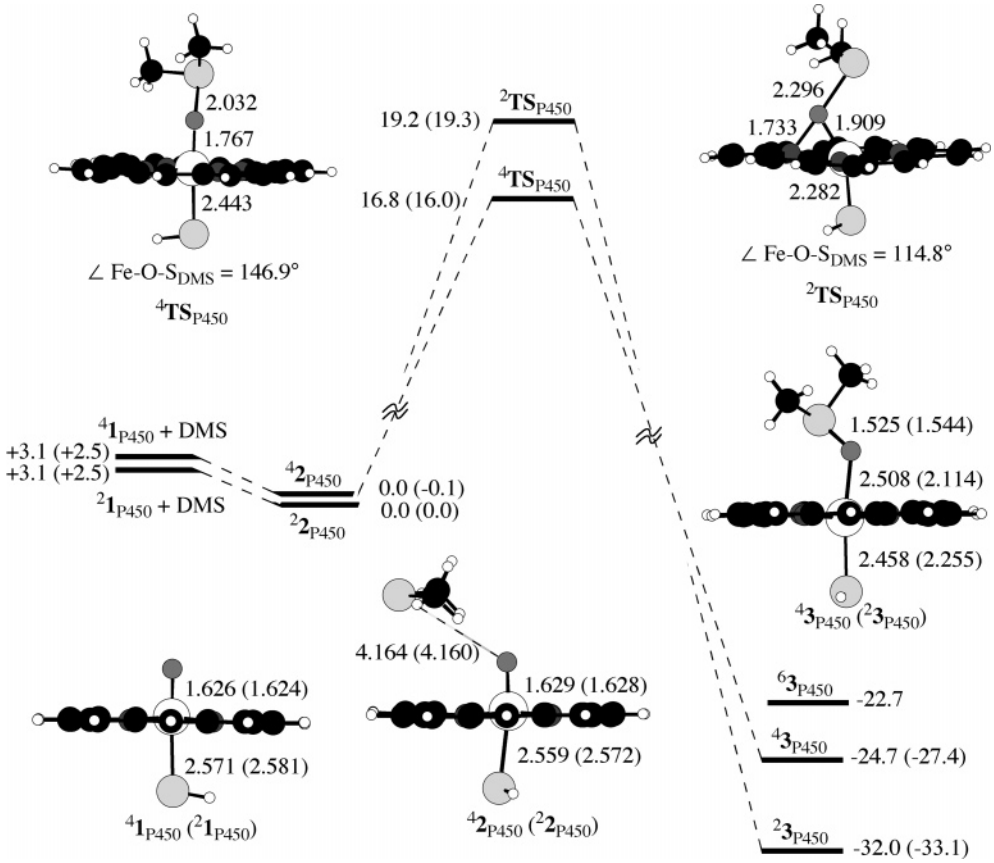

FIGURE 1: UB3LYP/LACVP** optimized geometries and relative energies (in kcal mol^{-1}) for the reaction of ^{4,2}Cpd I (P450) with DMS. Bond lengths are in Å. In parentheses the relative energies include medium correction, using a dielectric constant of $\epsilon = 5.7$. The superscripts to the left of the species designate the spin state. With the larger basis set, LACV3P^{+}*, the energy difference between the TSs increases to 5.5 kcal mol^{-1}; zero point energy and medium (using $\epsilon = 5.7$) corrections further increase this difference.

(P450) is 3.06 eV, while the one calculated for Cpd I (HRP) is 6.41 eV (*14*, *42*). We shall henceforth simply use the generic label a_{2u} to denote this orbital for the two species.

The set of orbitals in Scheme 2 is filled with 5 electrons in the electronic configuration $\delta^2\ \pi^*_{xz}{}^1\ \pi^*_{yz}{}^1\ a_{2u}{}^1$, which results in nearly degenerate quartet and doublet spin states. In the quartet state, the three unpaired electrons ($\pi^*_{xz}{}^1\ \pi^*_{yz}{}^1\ a_{2u}{}^1$) are ferromagnetically coupled, whereas in the doublet state they are antiferromagnetically coupled with a downspin electron in the a_{2u} orbital. The energy difference between these spin states may depend, however, on external factors such as hydrogen bonding or a polarized environment. Still, the aforementioned differences in electron affinities of the two species may change the reactivity pattern drastically.

Sulfoxidation by Cpd I (P450). Figure 1 shows the previously communicated (*46*) potential energy profile of direct oxygen transfer from Cpd I (P450), ^{4,2}**1**$_{P450}$, to DMS and optimized geometries of the critical points along the reaction path. Initially, a cluster complex (^{4,2}**2**$_{P450}$) is formed in which the hydrogen atoms of the methyl groups of DMS interact weakly with the negatively charged oxygen atom of the iron−oxo moiety. These clusters lead to a pair of

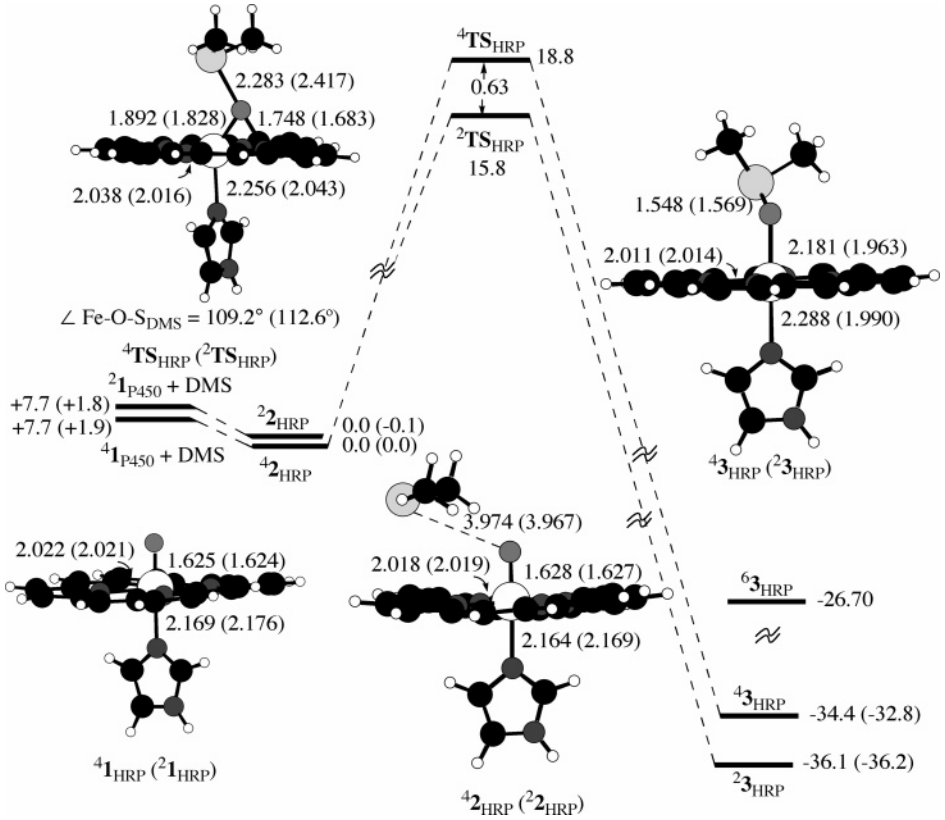

FIGURE 2: UB3LYP/LACVP** optimized geometries and relative energies for the reaction of ^{4,2}Cpd I (HRP) with DMS. All energies are in kcal mol^{-1}, and bond lengths are in Å. The superscripts to the left of the species correspond to the spin states. The geometries of ^{4,2}**1** are taken from de Visser et al. (*14*). In parentheses the relative energies correspond to a dielectric environment with a dielectric constant of $\epsilon = 5.7$. The energy datum, shown in between the ^{4,2}**TS**$_{HRP}$ species, corresponds to the best estimate at the LACV3P++**//LACVP** level with ZPE and correction for a medium with a dielectric constant of $\epsilon = 5.7$.

transition states (^{4,2}**TS**$_{P450}$) and subsequently to the sulfoxide product complexes (^{4,2}**3**$_{P450}$). A ^{6}**3**$_{P450}$ sextet-spin species is higher in energy as shown in the figure; the structure of the corresponding species is not depicted (*46*). As can be seen from Figure 1, the lowest-lying pathway occurs on the high-spin surface (the quartet spin), which has a 2.4 kcal mol^{-1} lower reaction barrier than the low-spin (the doublet spin) pathway. This difference increases when the effect of a dielectric medium (with a dielectric constant of $\epsilon = 5.7$) is used; the inclusion of hydrogen-bonding effect to the thiolate (*12*) does not change this difference (*46*). However, it increases to 5.5 kcal mol^{-1} when the basis set is further upgraded (*46*) (to the triple-ζ polarized basis set with diffuse functions on the heavy atoms, LACV3P$^+$*), and further to 6.9 kcal mol^{-1} when ZPE and medium effects are added to the results of the larger basis set. Thus, the computational data show a clear trend that the low-spin pathway is significantly higher than the high-spin one. This state ordering, i.e., ^{4}**TS**$_{P450}$ versus ^{2}**TS**$_{P450}$, is opposite to the state ordering that we obtained for the C−H hydrogen-abstraction reactions of Cpd I, for eleven different substrates, where the low-spin pathways were on average lower lying by 0.7 kcal mol^{-1} with ZPE correction (*43*, *44*, *51*).

Geometrically, ^{4}**TS**$_{P450}$ and ^{2}**TS**$_{P450}$ are very different. First, the Fe−S distance is elongated in the ^{4}**TS**$_{P450}$ due to the occupation of the $\sigma^*_{z^2}$ orbital with one electron. Second, the Fe−O−S angle is larger in the high-spin (HS) species (146.9°) compared with the much smaller angle in the low-spin (LS) species (114.8°). Moreover, in ^{2}**TS**$_{P450}$ the Fe−O bond is bent toward the porphine macrocycle, generating a relatively short O−N$_{Por}$ distance, which looks like a bond. These types of O-bridged complexes have been experimentally detected and characterized, and it is believed that they are extremely stable entities (*52*, *53*). However, here this geometric feature is restricted to the transition state and is absent in the sulfoxide product complexes, which exhibit a normal Fe−O bond between the heme and the dimethyl sulfoxide.

An Electron Transfer Mediated Sulfoxidation Mechanism by Cpd I (HRP). On the basis of the results by Goto et al. (*31*), we tested a mechanism with an initial electron transfer from the substrate to Cpd I. We started with the clusters between DMS and Cpd I (HRP), ^{4,2}**2**$_{HRP}$, and swapped the orbitals to yield a cluster of Cpd II and DMS$^{+\bullet}$. This state, however, was energetically high lying, and its wave function did not converge, falling back to Cpd I and DMS. This is reasonable since the ionization energy of DMS = 8.73 eV (B3LYP/6-31G) or 8.69 ± 0.02 eV (NIST) (*54*), whereas the electron affinity of Cpd I (HRP) is calculated to be significantly smaller, 6.41 eV (*14*). However, with other substrates, which have much lower ionization energy than DMS, an initial electron transfer may be entirely possible. This issue was not tested any further, and the sulfoxidation mechanism was henceforth followed as described below.

Sulfoxidation by Cpd I (HRP). Figure 2 displays the potential energy profile and critical species for the sulfoxidation of DMS by the model Cpd I (HRP) species. The formation of long-range complexes (^{4,2}**2**$_{HRP}$), from the isolated reactants, is accompanied by considerable shortening of the Fe−N$_{ImH}$ bond, by 0.072 Å, and elongation of the Fe−O

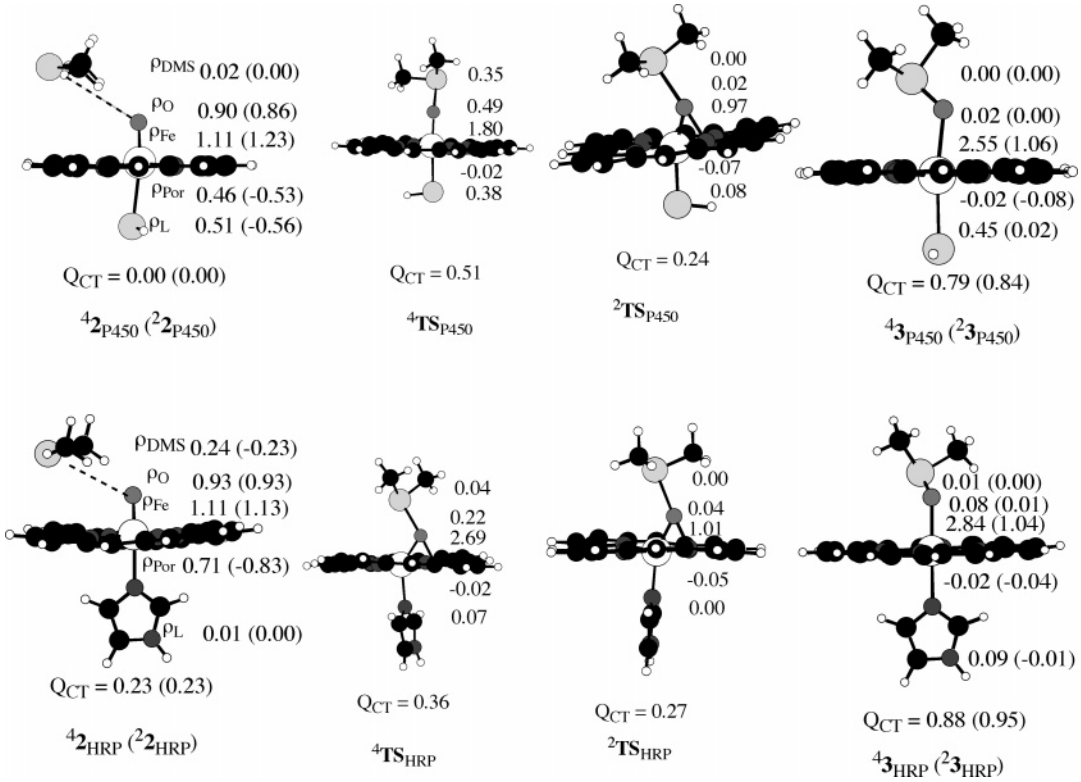

FIGURE 3: Group spin densities (ρ) in ^{4,2}**2**, ^{4,2}**TS**, and ^{2,4}**3**; the upper series correspond to the species in the P450 reaction, the lower series to the reaction of HRP. The superscript to the left of the species indicates the corresponding spin state. The order of the ρ data, from the top to the bottom moieties, is indicated for the first species in each series. The charge-transfer quantity Q_{CT} below the structures corresponds to the degree of charge transfer from dimethyl sulfide (DMS) to the oxo-heme moiety.

bond, by 0.040−0.042 Å. This is in contrast to P450, where only minor geometric differences were obtained between ^{4,2}**1**$_{P450}$ and ^{4,2}**2**$_{P450}$ (see Figure 1).

Still in contrast with the P450 case, where the high-spin path dominates the mechanism, here the situation is different. At the LACVP** level, ^{2}**TS**$_{HRP}$ lies 3.0 kcal mol^{-1} lower than ^{4}**TS**$_{HRP}$ (2.2 kcal mol^{-1} with ZPE correction); a dielectric medium increases the energy difference by ca. 1.2 kcal mol^{-1}. However, unlike the P450 case, here a single-point calculation with the larger basis set, LACV3P^{+}**, decreases this difference to 0.68 kcal mol^{-1} (in favor of the HS species). Shifting to a still larger basis set, LACV3P++** maintains the small energy difference of 0.63 kcal mol^{-1} (in favor of the LS species). Inclusion of ZPE correction further reduces the gap to 0.21 kcal mol^{-1} in favor of the HS species. Our best estimate at the level of LACV3P++**//LACVP** with ZPE correction and medium effect is 0.63 kcal mol^{-1} in favor of the LS transition state, ^{2}**TS**$_{HRP}$. Thus, *theory shows convergence of the computational data on a small energy difference between the two transition states*. This closeness in energy makes also a chemical sense in view of the very similar geometry of the two species (see below). This small energy difference is very similar to the findings in C−H hydroxylation (*51*). As such, much like in C−H hydroxylation, here too in sulfoxidation by HRP Cpd I, we expect the reactions to proceed by two-state reactivity (TSR) and to involve the two spin states. By contrast, in sulfoxidation by Cpd I (P450) there is a clear preference for reaction through the high-spin state.

Another pronounced difference compared with the P450 mechanism is in the geometry of the respective transition states. While ^{4}**TS**$_{P450}$ has an upright geometry and ^{2}**TS**$_{P450}$ a bent one, here ^{4}**TS**$_{HRP}$ and ^{2}**TS**$_{HRP}$ are similar with a strongly bent Fe−O bond that forms an O−N bond with the porphine. These O−N bonds vanish in the corresponding sulfoxide complexes, ^{4,2}**3**$_{HRP}$.

Electronic Structural Changes during Sulfoxidation. Some insight into the changes of electronic structure during sulfoxidation can be gained by inspection of the evolution of spin density (ρ) distribution along the four pathways, in Figure 3. Comparison of the reactant clusters, **2**, shows that with Cpd I (HRP) there is an early development of charge transfer from DMS to Cpd I, as indicated by the significant spin densities on the DMS moiety in ^{4,2}**2**$_{HRP}$, compared with almost zero in ^{4,2}**2**$_{P450}$. The same information is provided by the charge distribution, which shows that the amount of charge transfer, the Q_{CT} quantity, is significant for ^{4,2}**2**$_{HRP}$ and zero for ^{4,2}**2**$_{P450}$. Furthermore, the Q_{CT} quantities gradually increase in both mechanisms and converge to approximately one unit of charge that is transferred from DMS to the oxo−heme moiety at the product stage.

A closer inspection of the products, **3**, reveals that the iron atoms in the low-spin product complexes for P450 and HRP possess approximately one net spin, while the high-spin products have large densities on the iron atom, $\rho > 2.5$, namely, close to three electrons. In all the transition states and product complexes, the porphine macrocycle has virtually no spin density. Figure 3 further demonstrates that ^{2}**TS**$_{P450}$ has spin distribution similar to that of the respective product complex, ^{2}**3**$_{P450}$, and the same applies to ^{2}**TS**$_{HRP}$ and ^{4}**TS**$_{HRP}$, which share the spin density patterns of their respective products, ^{2}**3**$_{HRP}$ and ^{4}**3**$_{HRP}$. However, the high-spin species ^{4}**TS**$_{P450}$ is different; it has a significant spin density on the thiolate ligand and a significant spin on DMS, in

Scheme 3: Orbital Evolution Diagrams, from Reactants to Products, during Sulfoxidation of DMS by Cpd I (P450) and Cpd I (HRP)

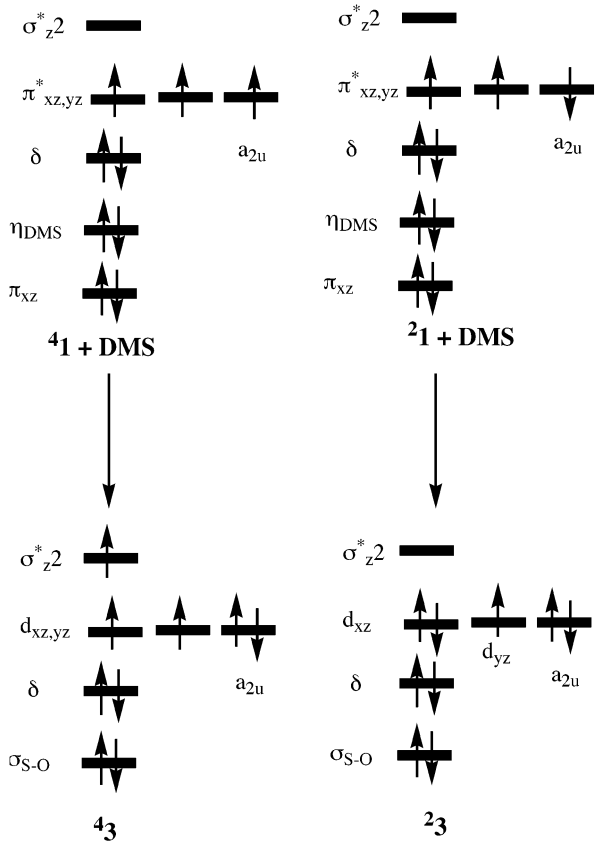

addition to its upright geometry. Generally, in most species, the spin density on the thiolate in the P450 reaction is always significant, in contrast to the dismal density on the imidazole in the HRP reaction.

This evolution of the spin density corresponds to the electronic structure changes, which are outlined in Scheme 3 using orbital energy diagrams for reactants and products. Thus, it is seen that the lone-pair orbitals, η_{DMS}, initially localized on DMS, and π_{xz} initially localized more on oxygen, combine and form the σ_{S-O} bond orbital in the dimethyl sulfoxide product. The π^*_{xz} and π^*_{yz} orbitals of the Fe═O moiety of Cpd I become more localized on the iron of the heme and are labeled as such, as d_{xz} and d_{yz} orbitals.

In each spin manifold in Scheme 3, the "iron configuration" is seen to change from d^4 ($\delta^2\pi^{*2}$) to d^5 ($\delta^2\pi^{*3}$ or $\delta^2\pi^{*2}\sigma^*_{z^2}{}^1$), thereby gaining one electron, and the a_{2u} orbital of the porphine-proximal ligand moiety gets filled. Thus, during the oxidation, in the LS manifold, the π^*_{xz} orbital of the FeO changes to d_{xz} and gains one electron, whereas during the oxidation on the HS manifold it is the $\sigma^*_{z^2}$ orbital that gains an electron; in both manifolds the a_{2u} orbital gains one electron. As such, the main orbitals that participate in the electronic reorganization are η_{DMS}, a_{2u}, π^*_{xz}, and $\sigma^*_{z^2}$.

A major difference between Cpd I (P450) and Cpd I (HRP) is the "involvement" of the thiolate in the electronic structure. This involvement is reflected in the high contribution of the thiolate to the key orbitals, as exemplified in Scheme 4, using the a_{2u} and $\sigma^*_{z^2}$ orbitals of the respective Cpd I species. Thus, it is seen that the a_{2u} and $\sigma^*_{z^2}$ orbitals, especially the former, are more delocalized onto the proximal ligand in the P450 species compared with the HRP species, where these orbitals are quite localized and contain dismal imidazole contribution. This difference between the two ligands reflects their relative electron-donation and iron-binding capabilities (*13a*).

Scheme 4: Key Orbital Differences for Cpd I (P450) and Cpd I (HRP) and for the Respective Transition States for Sulfoxidation, $^4TS_{P450}$ and $^4TS_{HRP}$[a]

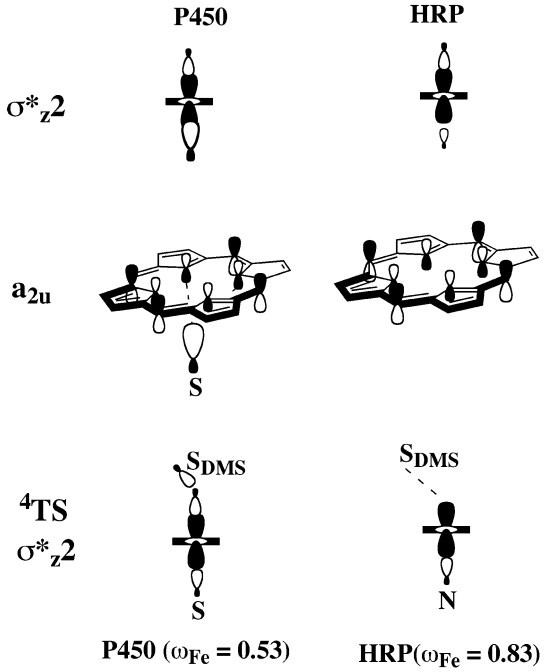

[a] The size of the sulfur and imidazole lobes reflects the relative contributions of the ligand to the respective orbitals. Similarly, the ω(Fe) quantity denotes the fractional weight of the Fe contribution to the $\sigma^*_{z^2}$ orbitals of the two ^{4}**TS** species.

The electronic structures and orbital shapes in the transition states are more complex than in Cpd I, but basically the above features carry over to these species too; there is a greater participation of thiolate ligand in the TS orbitals that are derived from a_{2u} and $\sigma^*_{z^2}$, compared with the imidazole ligand (see Supporting Information). For example, the contribution of iron to the $\sigma^*_{z^2}$ orbital, given by the fractional weight ω(Fe), is much smaller for the case of P450 due to the participation of the thiolate ligand in this orbital. Furthermore, the $\sigma^*_{z^2}$ (^{4}**TS**$_{P450}$) orbital is especially striking since it exhibits *a continuous delocalization over the S−Fe−O−S$_{DMS}$ moiety*. As can be seen from Scheme 4, this continuity is disrupted (no contribution on the DMS moiety) in ^{4}**TS**$_{HRP}$ where the proximal ligand is imidazole.

DISCUSSION

The computational results, on the "bare" Cpd I species, demonstrate that *there is a ligand-dependent spin selection of the preferred pathways as well as of the geometry of the respective transition states.* In the P450 reaction (Figure 1), the HS process is preferred and the corresponding ^{4}**TS**$_{P450}$ species has an upright geometry, while the LS ^{2}**TS**$_{P450}$ species has a highly distorted geometry with a bent Fe−O moiety having incipient O−N_{Por} bonding. By contrast, in the HRP reaction (Figure 3) the two transition states have the same geometry type and are therefore virtually degenerate in energy. Thus, sulfoxidation by HRP Cpd I is expected to proceed by two-state reactivity (TSR), while the reaction by

Scheme 5: Electron Filling of the Heme Orbitals and Overlap Cartoons[a]

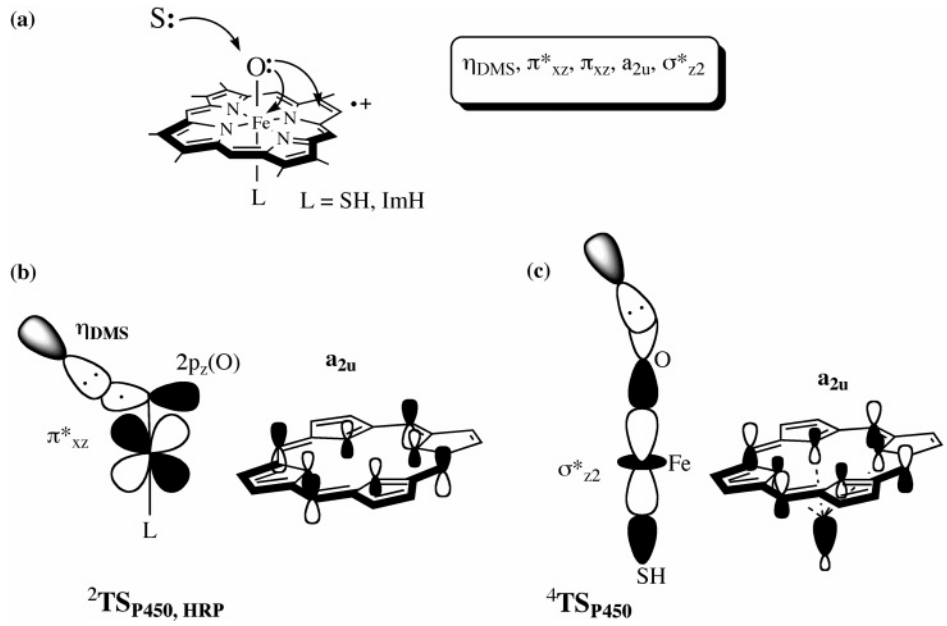

[a] (a) The electron filling of the heme orbitals during the sulfoxidation pathway, and the orbitals involved in the "electron flow". (b) An overlap cartoon for the three-electron $\eta_{DMS}-\pi^*_{xz}$ interaction. Note that, in order to relay one electron from these orbitals to a_{2u}, the $2p_z(O)$ lobe has to bend to overlap efficiently with the a_{2u} lobe orbitals on the nitrogens of the porphine. The requisite efficient overlap is achieved by Fe−O bending toward the porphine. (c) An overlap cartoon for the two-electron $\eta_{DMS}-\sigma^*_{z^2}$ interaction in the ^{4}**TS**$_{P450}$ species. Note that for this species the $\sigma^*_{z^2}$ and a_{2u} orbitals share a significant thiolate (SH^-) contribution. The corresponding a_{2u} orbital of the ^{4}**TS**$_{HRP}$ species is devoid of proximal ligand contribution.

P450 Cpd I will prefer single-state reactivity on the HS manifold (*55, 56*). We aim to comprehend this intriguing spin-state selectivity induced by the proximal ligand of the "bare" Cpd I species without the interference of the protein.

The electronic structures summarized above, in Scheme 3, reveal that the ferric complexes of the products, involve two oxidation equivalents lower than the respective reactant complexes. This is true as well for other oxidative processes of Cpd I, e.g., C−H hydroxylation where the electron filling of the heme orbitals occurs in two distinct steps corresponding to stepwise or nonsynchronous mechanisms (*56*). However, since the sulfoxidation reaction occurs in a single step (Figures 1 and 2), the two electrons that will fill the heme orbitals (Scheme 3) must be shifted also in a single step. Scheme 5a shows by the arrows the direction of the electron "flow", and indicates in the box the key orbitals that must be involved to effect this one-step reorganization. On the LS surface, these are the η_{DMS}, π^*_{xz} (in combination with π_{xz}), and a_{2u} orbitals, whereas on the HS surface the interaction of η_{DMS} with the $\sigma^*_{z^2}$ and a_{2u} orbitals is involved. Other orbitals will necessarily be affected, but for the sake of relative simplicity, we disregard them and use the minimal set of orbitals in Scheme 5. A more detailed picture using orbital interaction diagrams is given in the Appendix.

At the outset, it is clear that the structures and hence also the energies of the respective transition states must reflect in each case the most efficient overlaps of these orbitals; *some sort of "overlap continuity" would be the desirable situation that optimizes the bonding in the TS*. Scheme 5b,c show these orbital interactions using simple overlap cartoons. In the low-spin mechanisms of both HRP and P450, in Scheme 5b, the key interacting orbitals are η_{DMS}, π^*_{xz}, and a_{2u}; to save space, the latter orbital is commonly depicted for the HRP and P450 ^{2}**TS** species. The $\eta_{DMS}-\pi^*_{xz}$ interaction is a three-electron interaction that is maximized in a sideways attack of DMS on the FeO moiety; two electrons will be stabilized in the bonding-combination orbital, and the third that has to populate the antibonding-combination orbital will be relayed to the a_{2u} orbital, which in Cpd I is singly occupied. This requires some overlap between the $2p_z$ lobe on the oxygen of the oxo−iron moiety and the a_{2u} orbital. Since the latter orbital is largely located on the nitrogen atoms of the porphine, the Fe−O moiety has to bend toward one of the porphine nitrogen atoms to achieve some O−N overlap. This is the reason why the low-spin ^{2}**TS**$_{P450}$ and ^{2}**TS**$_{HRP}$ have a bent Fe−O moiety (Figures 1 and 2), and why the porphine loses its spin density in the two transition states (Figure 3).

In the high-spin transition state, ^{4}**TS**$_{P450}$, in Scheme 5c, the key orbital interactions involve η_{DMS}, $\sigma^*_{z^2}$, and a_{2u}. The η_{DMS}-$\sigma^*_{z^2}$ *orbital overlap requires an almost upright conformation* (Figure 1). This is a two-electron interaction, and only one of these electrons will remain in $\sigma^*_{z^2}$; the other will have to be relayed to a_{2u}. In fact, the $\sigma^*_{z^2}$ and a_{2u} orbitals can maintain an efficient coupling since they share a significant contribution from the thiolate hybrid orbital (see Scheme 5c and also the corresponding orbitals in Scheme 4). Thus, the electron relay to the a_{2u} orbital can efficiently occur in this upright conformation without a need for bending. This is the reason why ^{4}**TS**$_{P450}$ is more stable than its LS counterpart species, ^{2}**TS**$_{P450}$, and having an almost upright conformation as opposed to the bent and sideways conformation of ^{2}**TS**$_{P450}$ (Figure 1).

The situation in the ^{4}**TS**$_{HRP}$ species is very different; here the imidazole orbitals do not mix with the a_{2u} orbital and have only small mixing with $\sigma^*_{z^2}$ (Scheme 4). As a result, the a_{2u} and $\sigma^*_{z^2}$ orbitals remain disjointed, and *the advantage of the upright conformation is lost*. Consequently, the ^{4}**TS**$_{HRP}$ species resorts to the $\eta_{DMS}-\pi^*_{xz}$ three-electron interaction to relay the electrons to a_{2u} and to $\sigma^*_{z^2}$. This is the reason

why now the structure of ^{4}**TS**$_{HRP}$ involves a bent Fe−O bond and O−N$_{Por}$ bonding, much like the low-spin counterpart, ^{2}**TS**$_{HRP}$, species. Since the two transition states are isostructural, the significant energy advantage encountered on the HS path in the P450 reaction is lost here, and the ^{2}**TS**$_{HRP}$ and ^{4}**TS**$_{HRP}$ species attain similar energies as in a TSR scenario (*55*, *56*).

Thus, in a nutshell, the sulfoxidation mechanisms follow simple *orbital-selection rules*, which are strongly dependent upon the identity of the proximal ligand. In the case of thiolate, the mechanism prefers the HS pathway, and the corresponding ^{4}**TS**$_{P450}$ species has a strong charge-transfer character (Figure 3). By contrast, in the case of imidazole, the preferred mechanism is TSR, where both HS and LS pathways contribute. Furthermore, with thiolate, the HS transition state, ^{4}**TS**$_{P450}$, has an upright conformation with a large Fe−O−S$_{DMS}$ angle of 147°, whereas the LS species, ^{2}**TS**$_{P450}$, has a small angle and its Fe−O bond makes an O−N bond with the porphine. However, when the proximal ligand is imidazole, both transition states possess a bent Fe−O bond and an O−N$_{Por}$ bond. *These intriguing results indicate that there is a ligand-dependent spin selection of the pathway as well as of the structure of the respective transition states.* This is a beautiful example how the electronic properties of the ligand (e.g., "push effect" of the thiolate (*4*, *11*), vis-à-vis electron withdrawal by the imidazole (*4*, *12*)) are translated into a mechanistic selection. In contrast to these differences, the relative barrier heights do not seem to be dependent greatly on the axial ligand; as such, sulfoxidation by HRP should be intrinsically as facile as by P450, had it not been for the steric constraints of the protein pocket. Experimentally, HRP is known to be a reasonably good effector of sulfoxidation (*28*, *29*).

In the general situation, the sulfoxidation reaction catalyzed by heme-enzymes will be expected to depend on the HS/LS ratio and/or interconversion rate of the spin states of Cpd I, and on the possibility of spin crossover during the reaction process. However, the spin selection may have other intriguing experimental consequences in cases where a substrate has two oxidizable moieties, one proceeding via TSR where the two spin pathways are close and competitive, the other by one of the spin states. As was argued by Jones et al. (*57*), reiterated by us (*46*, *58*), and reinforced again by the Jones group (*59*), the competition of N-dealkylation and sulfoxidation by P450 enzymes may belong to these cases where the different moieties are oxidized via different spin manifolds, *which disguise as two different oxidants*.

Conclusions and Summary. The sulfoxidation mechanisms of dimethyl sulfide (DMS) by the HRP and P450 enzymes differ intrinsically in the identity of the axial ligand: thiolate in P450 and imidazole in HRP. Models of these two enzymes show that the respective active species, compound I (Cpd I), exhibit spin-selective reactivity that is dependent on the axial ligand. Cpd I of P450 exhibits preference for a high-spin (HS) reactivity, whereas Cpd I of HRP exhibits no clear preference and, hence, is likely to proceed by two-state reactivity (TSR). The HS transition state in the P450 mechanism, ^{4}**TS**$_{P450}$, involves an upright orientation of the dimethyl sulfide (DMS) with respect to the S−Fe−O axis of Cpd I, whereas the low-spin (LS) transition state, ^{2}**TS**$_{P450}$, has a small Fe−O−S$_{DMS}$ angle and its Fe−O bond is bent toward the porphyrin, as though there is an O−N$_{Por}$ bond. By contrast, in the HRP mechanism both HS and LS transition states have a small Fe−O−S$_{DMS}$ angle and a bent Fe−O bond. Otherwise, in both enzymes the sulfoxidation processes from either spin state are concerted single-step reactions. The relative barriers show that *intrinsically*, without the effect of the protein pocket constraints, HRP is as reactive as P450 toward hydroxylation.

The different *mechanistic features of the two enzymes follow orbital-selection rules*, due to the interaction of the DMS orbital (η_{DMS}) with the a_{2u}, $\sigma^*_{z^2}$, and π^*_{xz} orbitals of the oxo−iron porphyrin (oxo-heme) reagent. The geometry and spin selection derive from the different involvement of the ligand orbitals in the key oxo-heme orbitals; the oxo-heme orbitals involve significant mixing with the thiolate ligand but not with imidazole. The preferred orbital interaction in the HS species, ^{4}**TS**, is the one between η_{DMS} and $\sigma^*_{z^2}$ and a_{2u}, which favors an upright conformation as long as there is overlap continuity between the interacting orbitals. Thus, the mixing of the thiolate ligand of P450 into both the a_{2u} and $\sigma^*_{z^2}$ orbitals creates overlap continuity and, hence, a preference for the HS pathway and for an upright orientation in the corresponding transition-state species, ^{4}**TS**$_{P450}$. The preferred orbital interaction in the LS transition state is the one between η_{DMS} and π^*_{xz} and a_{2u}, which forces a sideways attack and a bending of the Fe−O bond toward the porphine. The poor mixing of the imidazole orbitals into the oxo-heme orbitals cancels the HS advantage in the upright orientation, enforces mixing with the π^*_{xz} orbital, and creates similar geometry for the two transition-state species, ^{4}**TS**$_{HRP}$ and ^{2}**TS**$_{HRP}$; both species now have a bent Fe−O bond with O−N$_{Por}$ bonding. These orbital-mixing patterns (see Appendix) are manifestations of the fact that thiolate is a powerful electron donor and a good iron binder compared with imidazole.

Of course, the above trends do not involve the effect of the protein, which may or may not alter the structural characteristics of the transition state species reported in this study. This will have to be examined by hybrid QM/MM calculations. In case it is found that the protein alters the intrinsic trends, one may then attempt to design appropriate mutants that can accommodate the intrinsic preferences of these species. If, however, the protein retains the intrinsic characteristics, then the work described here forms a predictive basis for mechanistic research.

APPENDIX

Scheme 6 complements Scheme 5 and shows schematic and simplified orbital interaction diagrams of DMS with Cpd I, for two different modes of attack. Part a corresponds to a sideways attack of DMS and shows the three-electron interaction of the DMS lone pair (η_{DMS}) with the π^*_{xz} orbital of Cpd I. Two of the electrons end up in the σ_{S-O} orbital of the sulfoxide, while the third electron is relayed to the a_{2u} orbital. Note that the three-orbital interaction—η_{DMS}, π^*_{xz}, and π_{xz}—causes localization of the 2p lone pair on oxygen, and a d_{xz} orbital on Fe. In turn, the 2p(O) orbital overlaps with the DMS orbital and forms the σ_{S-O} bond orbital. Part b corresponds to an upright attack, and shows the two-electron interaction of η_{DMS} with the $\sigma^*_{z^2}$ orbital and the filling of the a_{2u} orbital. In both cases the electron pair in the a_{2u} orbital of the TS is shown in parentheses.

Scheme 6

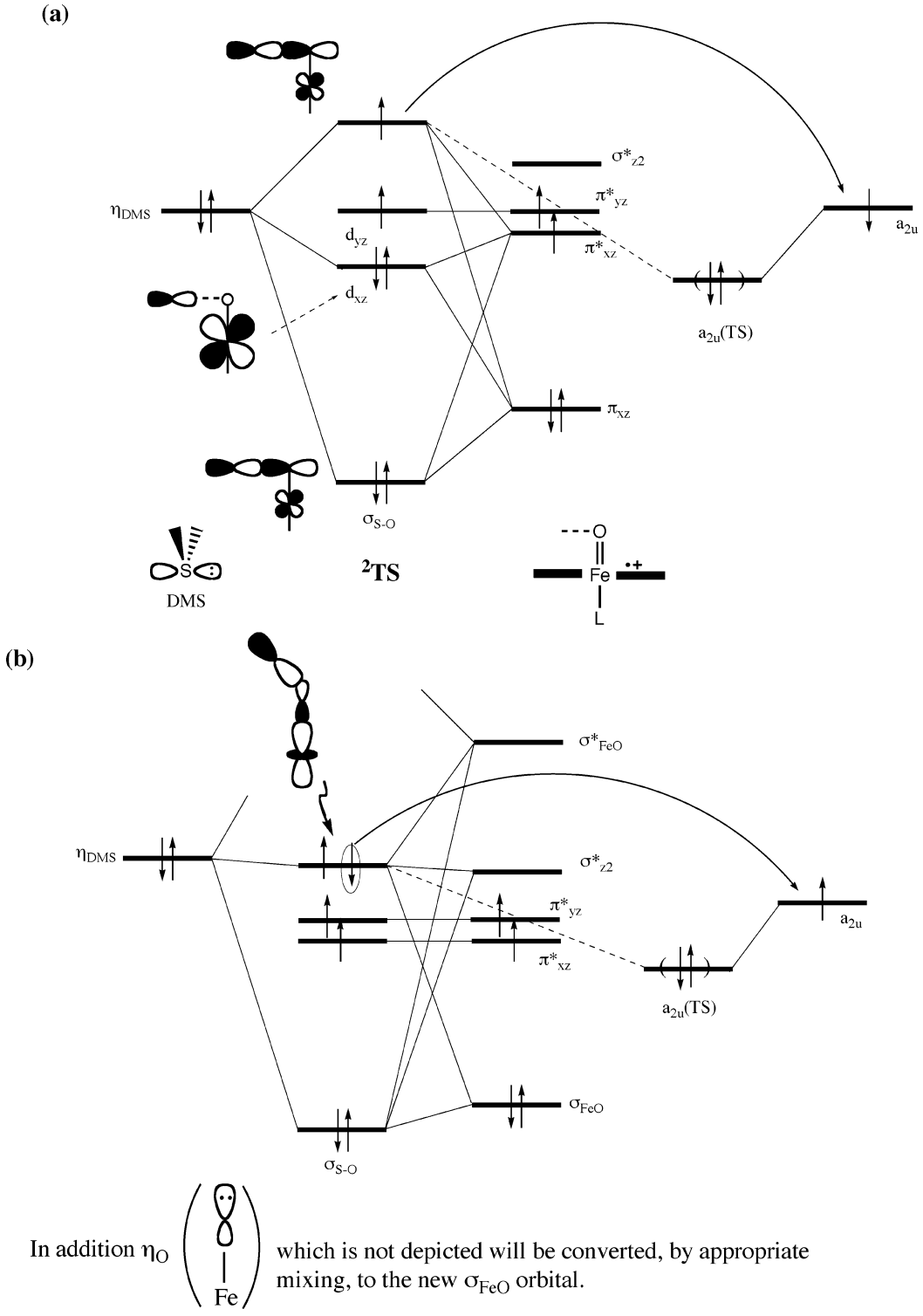

SUPPORTING INFORMATION AVAILABLE

Eleven tables and 8 figures with computational data such as absolute energies, charges, and spin densities of all optimized structures under different environmental conditions. This material is available free of charge via the Internet at http://pubs.acs.org.

REFERENCES

1. (a) Ortiz de Montellano, P. R., Ed. (1995) *Cytochrome P450: Structure, Mechanisms, and Biochemistry*, 2nd ed., Plenum Press, New York. (b) Ortiz de Montellano, P. R., Ed. (2004) *Cytochrome P450: Structure, Mechanisms, and Biochemistry*, 3rd ed., Plenum Press, New York. (c) Kadish, K. M., Smith, K. M., and Guilard, R., Eds. (2000) *The Porphyrin Handbook*, Academic Press, San Diego, CA.
2. Ortiz de Montellano, P. R., and De Voss, J. J. (2002) Oxidizing species in the mechanism of cytochrome P450, *Nat. Prod. Rep. 19*, 477−493.
3. (a) Woggon, W.-D. (1997) Cytochrome P450: significance, reaction mechanisms and active site analogs, *Top. Curr. Chem. 184*, 39−96. (b) Woggon, W.-D., Wagenknecht, H.-A., and Claude, C. (2001) Synthetic active site analogues of heme-thiolate proteins. Characterization and identification of intermediates of

the catalytic cycles of cytochrome $P450_{cam}$ and chloroperoxidase, *J. Inorg. Biochem. 83*, 289−300.
4. Sono, M., Roach, M. P., Coulter, E. D., and Dawson, J. H. (1996) Heme-Containing Oxygenases, *Chem. Rev. 96*, 2841−2887.
5. (a) Groves, J. T. (1985) Key elements of the chemistry of cytochrome P-450. The oxygen rebound mechanism, *J. Chem. Educ. 62*, 928−931. (b) Groves, J. T. (2003) The bioinorganic chemistry of iron in oxygenases and supramolecular assemblies, *Proc. Natl. Acad. Sci. U.S.A. 100*, 3569−3574.
6. Guengerich, F. P. (2001) Common and uncommon cytochrome P450 reactions related to metabolism and chemical toxicity, *Chem. Res. Toxicol. 14*, 611−650.
7. Meunier, B., and Bernadou, J. (2002) Metal-oxo species in P450 enzymes and biomimetic models. Oxo-hydroxo tautomerism with water-soluble metalloporphyrins, *Top. Catal. 21*, 47−55.
8. (a) Poulos, T. L. (2000) in *The Porphyrin Handbook* (Kadish, K. M., Smith, K. M., and Guilard, R., Eds.) Vol. 4, Chapter 32, pp 189−218, Academic Press, San Diego, CA. (b) Poulos, T. L., Cupp-Vickery, J., and Li, H. (1995) in *Cytochrome P450: Structure, Mechanisms, and Biochemistry* (Ortiz de Montellano, P. R., Ed.) 2nd ed., Chapter 4, pp 125−150, Plenum Press, New York.
9. Schlichting, I., Berendzen, J., Chu, K., Stock, A. M., Maves, S. A., Benson, D. E., Sweet, R. M., Ringe, D., Petsko, G. A., and Sligar, S. G. (2000) The catalytic pathway of cytochrome $P450_{cam}$ at atomic resolution, *Science 287*, 1615−1622.
10. Berglund, G. I., Carlsson, G. H., Smith, A. T., Szöke, H., Henriksen, A., and Hajdu, J. (2002) The catalytic pathway of horseradish peroxidase at high resolution, *Nature 417*, 463−468.
11. Dawson, J. H., Holm, R. H., Trudell, J. R., Barth, G., Linder, R. E., Bunnenberg, E., Djerassi, C., and Tang, S. C. (1976) Oxidized cytochrome P-450. Magnetic circular dichroism evidence for thiolate ligation in the substrate-bound form. Implications for the catalytic mechanism, *J. Am. Chem. Soc. 98*, 3707−3709.
12. Poulos, T. L. (1996) The role of the proximal ligand in heme enzymes, *J. Biol. Inorg. Chem. 1*, 356−359.
13. For computational investigations of the electron releasing effect of thiolate, see: (a) Ogliaro, F., de Visser, S. P., and Shaik, S. (2002) The 'push' effect of the thiolate ligand in cytochromeP450: a theoretical gauging, *J. Inorg. Biochem. 91*, 554−567. (b) Rydberg, P., Sigfridsson, E., and Ryde, U. (2004) On the role of the axial ligand in heme proteins: a theoretical study, *J. Biol. Inorg. Chem. 9*, 203−223.
14. de Visser, S. P., Shaik, S., Sharma, P. K., Kumar, D., and Thiel, W. (2003) Active species of horseradish peroxidase (HRP) and cytochrome P450: two electronic chameleons, *J. Am. Chem. Soc. 125*, 15779−15788.
15. For general reviews on Compound I species, see: (a) Harris, D. L. (2001) High-valent intermediates of heme proteins and model compounds, *Curr. Opin. Chem. Biol. 5*, 724−735. (b) Harris, D. L., and Loew, G. H. (2001) Proximal ligand effects on electronic structure and spectra of compound I of peroxidases, *J. Porphyrins Phthalocyanines 5*, 334−344. (c) Loew, G. H., and Harris, D. L. (2000) Role of the heme active site and protein environment in structure, spectra, and function of the cytochrome P450s, *Chem. Rev. 100*, 407−419.
16. Wirstam, M., Blomberg, M. R. A., and Siegbahn, P. E. M. (1999) Reaction mechanism of compound I formation in heme peroxidases: a density functional theory study, *J. Am. Chem. Soc. 121*, 10178−10185.
17. Benecky, M. J., Frew, J. E., Scowen, N., Jones, P., and Hoffman, B. M. (1993) EPR and ENDOR detection of compound I from *Micrococcus lysodeikticus* catalase, *Biochemistry 32*, 11929−11933.
18. Loew, G. H., Kert, C. J., Hjelmeland, L. M., and Kirchner, R. F. (1977) Active site models of horseradish peroxidase compound I and a cytochrome P-450 analogue: electronic structure and electric field gradients, *J. Am. Chem. Soc. 99*, 3534−3536.
19. Du, P., and Loew, G. H. (1995) Theoretical study of model compound I complexes of horseradish peroxidase and catalase, *Biophys. J. 68*, 69−80.
20. Kuramochi, H., Noodleman, L., and Case, D. A. (1997) Density functional study on the electronic structures of model peroxidase compounds I and II, *J. Am. Chem. Soc. 119*, 11442−11451.
21. Antony, J., Grodzicki, M., and Trautwein, A. X. (1997) Local density functional study of oxoiron(IV) porphyrin complexes and their one-electron oxidized derivatives. Axial ligand effects, *J. Phys. Chem. A 101*, 2692−2701.
22. Deeth, R. J. (1999) Saddle distortions of ferryl-porphyrin models for peroxidase compound I: a density functional study, *J. Am. Chem. Soc. 121*, 6074−6075.
23. Filatov, M., Harris, N., and Shaik, S. (1999) A theoretical study of electronic factors affecting hydroxylation by model ferryl complexes of cytochrome P-450 and horseradish peroxidase, *J. Chem. Soc., Perkin Trans. 2*, 399−410.
24. Green, M. T. (2000) Imidazole-ligated compound I intermediates: the effects of hydrogen bonding, *J. Am. Chem. Soc. 122*, 9495−9499.
25. Dawson, J. H. (1988) Probing structure-function relations in heme-containing oxygenases and peroxidases, *Science 240*, 433−439.
26. Pérez, U., and Dunford, H. B. (1990) Transient-state kinetics of the reactions of 1-methoxy-4-(methylthio)benzene with horseradish peroxidase compounds I and II, *Biochemistry 29*, 2757−2763.
27. Doerge, D. R., Cooray, N. M., and Brewster, M. E. (1991) Peroxidase-catalyzed S-oxygenation: mechanism of oxygen transfer for lactoperoxidase, *Biochemistry 30*, 8960−8964.
28. (a) Ozaki, S.-i., and Ortiz de Montellano, P. R. (1994) Molecular engineering of horseradish peroxidase. Highly enantioselective sulfoxidation of aryl alkyl sulfides by the Phe-41 → Leu mutant, *J. Am. Chem. Soc. 116*, 4487−4488. (b) Ozaki, S.-i., and Ortiz de Montellano, P. R. (1995) Molecular engineering of horseradish peroxidase: thioether sulfoxidation and styrene epoxidation by Phe-41 leucine and threonine mutants, *J. Am. Chem. Soc. 117*, 7056−7064. (c) Ortiz de Montellano, P. R. (1992) Catalytic sites of hemoprotein peroxidases, *Annu. Rev. Pharmacol. Toxicol. 32*, 89−107.
29. Ator, M. A., and Ortiz de Montellano, P. R. (1987) Protein control of prosthetic heme reactivity. Reaction of substrates with the heme edge of horseradish peroxidase, *J. Biol. Chem. 262*, 1542−1551.
30. Rietjens, I. M. C. M., Osman, A. M., Veeger, C., Zakharieva, O., Antony, J., Grodzicki, M., and Trautwein, A. X. (1996) On the role of the axial ligand in heme-based catalysis of the peroxidase and P450 type, *J. Biol. Inorg. Chem. 1*, 372−376.
31. Goto, Y., Matsui, T., Ozaki, S.-i., Watanabe, Y., and Fukuzumi, S. (1999) Mechanisms of sulfoxidation catalyzed by high-valent intermediates of heme enzymes: electron-transfer vs oxygen-transfer mechanism, *J. Am. Chem. Soc. 121*, 9497−9502.
32. Das, P. K., Caaveiro, J. M. M., Luque, S., and Klibanov, A. M. (2002) Binding of hydrophobic hydroxamic acids enhances peroxidase's stereoselectivity in nonaqueous sulfoxidations, *J. Am. Chem. Soc. 124*, 782−787.
33. Kato, S., Yang, H.-J., Ueno, T., Ozaki, S.-i., Phillips, G. N., Jr., Fukuzumi, S., and Watanabe, Y. (2002) Asymmetric sulfoxidation and amine binding by H64D/V68A and H64D/V68S Mb: mechanistic insight into the chiral discrimination step, *J. Am. Chem. Soc. 124*, 8506−8507.
34. Matsui, T., Nagano, S., Ishimori, K., Watanabe, Y., and Morishima, I. (1996) Preparation and reactions of myoglobin mutants bearing both proximal cysteine ligand and hydrophobic distal cavity: protein models for the active site of P-450, *Biochemistry 35*, 13118−13124.
35. Ozaki, S.-i., Matsui, T., and Watanabe, Y. (1997) Conversion of myoglobin into a peroxygenase: a catalytic intermediate of sulfoxidation and epoxidation by the F43H/H64L mutant, *J. Am. Chem. Soc. 119*, 6666−6667.
36. Suzuki, N., Huguchi, T., Urano, Y., Kikuchi, K., Uekusa, H., Ohashi, Y., Uchida, T., Kitagawa, T., and Nagano, T. (1999) Novel iron porphyrin-alkanethiolate complex with intramolecular NH···S hydrogen bond: synthesis, spectroscopy, and reactivity, *J. Am. Chem. Soc. 121*, 11571−11572.
37. Ohno, T., Suzuki, N., Dokoh, T., Urano, Y., Kikuchi, K., Hirobe, M., Higuchi, T., and Nagano, T. (2000) Remarkable axial thiolate ligand effect on the oxidation of hydrocarbons by active intermediate of iron porphyrin and cytochrome P450, *J. Inorg. Biochem. 82*, 123−125.
38. Nam, W., Lim, M. H., Oh, S.-Y., Lee, J. H., Lee, H. J., Woo, S. K., Kim, C., and Shin, W. (2000) Remarkable anionic axial ligand effects of iron(III) porphyrin complexes on the catalytic oxygenations of hydrocarbons by H_2O_2 and the formation of oxoiron(IV) porphyrin intermediates by *m*-chloroperoxybenzoic acid, *Angew. Chem., Int. Ed. 39*, 3646−3649.
39. Fruetel, J., Chang, Y.-T., Collins, J., Loew, G., and Ortiz de Montellano, P. R. (1994) Thioanisole sulfoxidation by cytochrome $P450_{cam}$ (CYP101): experimental and calculated absolute stereochemistries, *J. Am. Chem. Soc. 116*, 11643−11648.
40. Adam, W., Heckel, F., Saha-Möller, C. R., and Schreier, P. (2002) Biocatalytic synthesis of optically active oxyfunctionalized build-

ing blocks with enzymes, chemoenzymes and microorganisms, *J. Organomet. Chem. 661*, 17−29.
41. Baciocchi, E., Gerini, M. F., Lanzalunga, O., Lapi, A., and Piparo, M. G. L. (2003) Mechanism of the oxidation of aromatic sulfides catalysed by a water soluble iron porphyrin, *Org. Biomol. Chem. 1*, 422−426.
42. A recent study compares the intrinsic C−H hydroxylation and C═C epoxidation of the two species. See: Kumar, D., de Visser, S. P., Sharma, P. K., Derat, E., and Shaik, S. (2005) The intrinsic axial ligand effect on propene oxidation by horseradish peroxidase versus cytochrome P450 enzymes, *J. Biol. Inorg. Chem. 10*, 181−189.
43. de Visser, S. P., Ogliaro, F., Sharma, P. K., and Shaik, S. (2002) What factors affect the regioselectivity of oxidation by cytochrome P450? A DFT study of allylic hydroxylation and double bond epoxidation in a model reaction, *J. Am. Chem. Soc. 124*, 11809−11826.
44. Kumar, D., de Visser, S. P., Sharma, P. K., Cohen, S., and Shaik, S. (2004) Radical clock substrates, their C−H hydroxylation mechanism by cytochrome P450, and other reactivity patterns: what does theory reveal about the clocks' behavior? *J. Am. Chem. Soc. 126*, 1907−1920.
45. Ogliaro, F., de Visser, S. P., Cohen, S., Kaneti, J., and Shaik, S. (2001) The experimentally elusive oxidant of cytochrome P450: a theoretical "trapping" defining more closely the "real" species, *ChemBioChem 2*, 848−851.
46. Sharma, P. K., de Visser, S. P., and Shaik, S. (2003) Can a single oxidant with two spin states masquerade as two different oxidants? A study of the sulfoxidation mechanism by cytochrome P450, *J. Am. Chem. Soc. 125*, 8698−8699.
47. (a) Becke, A. D. (1992) Density-functional thermochemistry. I. The effect of the exchange-only gradient correction, *J. Chem. Phys. 96*, 2155−2160. (b) Becke, A. D. (1992) Density-functional thermochemistry. II. The effect of the Perdew-Wang generalized-gradient correlation correction, *J. Chem. Phys. 97*, 9173−9177. (c) Becke, A. D. (1993) Density-functional thermochemistry. III. The role of exact exchange, *J. Chem. Phys. 98*, 5648−5652. (d) Lee, C., Yang, W., and Parr, R. G. (1988) Development of the Colle-Salvetti correlation-energy formula into a functional of the electron density, *Phys. Rev. B 37*, 785−789.
48. Frisch, M. J., Trucks, G. W., Schlegel, H. B., Scuseria, G. E., Robb, M. A., Cheeseman, J. R., Zakrzewski, V. G., Montgomery, J. A., Jr., Stratmann, R. E., Burant, J. C., Dapprich, S., Millam, J. M., Daniels, A. D., Kudin, K. N., Strain, M. C., Farkas, O., Tomasi, J., Barone, V., Cossi, M., Cammi, R., Mennucci, B., Pomelli, C., Adamo, C., Clifford, S., Ochterski, J., Petersson, G. A., Ayala, P. Y., Cui, Q., Morokuma, K., Malick, D. K., Rabuck, A. D., Raghavachari, K., Foresman, J. B., Cioslowski, J., Ortiz, J. V., Baboul, A. G., Stefanov, B. B., Liu, G., Liashenko, A., Piskorz, P., Komaromi, I., Gomperts, R., Martin, R. L., Fox, D. J., Keith, T., Al-Laham, M. A., Peng, C. Y., Nanayakkara, A., Gonzalez, C., Challacombe, M., Gill, P. M. W., Johnson, B., Chen, W., Wong, M. W., Andres, J. L., Head-Gordon, M., Replogle, E. S., Pople, J. A. (1998) *Gaussian 98*, Gaussian, Inc., Pittsburgh, PA.
49. *Jaguar 4.2* (1991−2000) Schrödinger, Inc., Portland, OR.
50. (a) Hay, J. P., and Wadt, W. R. (1985) *Ab initio* effective core potentials for molecular calculations. Potentials for K to Au including the outermost core orbitals, *J. Chem. Phys. 82*, 299−310. (b) Friesner, R. A., Murphy, R. B., Beachy, M. D., Ringlanda, M. N., Pollard, W. T., Dunietz, B. D., and Cao, Y. (1999) Correlated ab initio electronic structure calculations for large molecules, *J. Phys. Chem. A 103*, 1913−1928.
51. de Visser, S. P., Kumar, D., Cohen, S., Shacham, R., and Shaik, S. (2004) A predictive pattern of computed barriers for C−H hydroxylation by compound I of cytochrome P450, *J. Am. Chem. Soc. 126*, 8362−8363.
52. Mizutani, Y., Watanabe, Y., and Kitagawa, T. (1994) Resonance Raman characterization of iron(III) porphyrin *N*-oxide: evidence for an Fe−O−N bridged structure, *J. Am. Chem. Soc. 116*, 3439−3441.
53. Watanabe, Y. (2001) Alternatives to the oxoferryl porphyrin cation radical as the proposed reactive intermediate of cytochrome P450: two-electron oxidized Fe(III) porphyrin derivatives, *J. Biol. Inorg. Chem. 6*, 846−856.
54. Linstrom, P. J., and Mallard, W. G., Eds. (2003) *NIST Chemistry WebBook*, NIST Standard Reference Database Number 69, March 2003, National Institute of Standards and Technology, Gaitherburg, MD 20899 (http://webbook.nist.gov).
55. (a) Shaik, S., Filatov, M., Schröder, D., and Schwarz, H. (1998) Electronic structure makes a difference: cytochrome P-450 mediated hydroxylation of hydrocarbons as a two-state reactivity paradigm, *Chem. Eur. J. 4*, 193−199. (b) Shaik, S., de Visser, S. P., Ogliaro, F., Schwarz, H., and Schröder, D. (2002) Two-state reactivity mechanisms of hydroxylation and epoxidation by cytochrome P-450 revealed by theory, *Curr. Opin. Chem. Biol. 6*, 556−567.
56. (a) Shaik, S., and de Visser, S. P. (2004) Computational approaches to cytochrome P450 function, in *Cytochrome P450: Structure, Mechanism, and Biochemistry* (Ortiz de Montellano, P. R., Ed.) 3rd ed., pp 45−85, Kluwer Academic/Plenum Publishers, New York. (b) Meunier, B., de Visser, S. P., and Shaik, S. (2004) Mechanism of oxidation reactions catalyzed by cytochrome P450 enzymes, *Chem. Rev. 104*, 3947−3980.
57. Volz, T. J., Rock, D. A., and Jones, J. P. (2002) Evidence for two different active oxygen species in cytochrome P450 BM3 mediated sulfoxidation and N-dealkylation reactions, *J. Am. Chem. Soc. 124*, 9724−9725.
58. Shaik, S., de Visser, S. P., and Kumar, D. (2004) One oxidant, many pathways: a theoretical perspective of monooxygenation mechanisms by cytochrome P450 enzymes, *J. Biol. Inorg. Chem. 9*, 661−668.
59. Dowers, T. S., Rock, D. A., Rock, D. A., and Jones, J. P. (2004) Kinetic isotope effects implicate the iron-oxene as the sole oxidant in P450-catalyzed N-dealkylation, *J. Am. Chem. Soc. 126*, 8868−8869.

BI050348C